

Angular dependence and symmetry of Rashba spin torque in ferromagnetic heterostructures

Christian Ortiz Pauyac,¹ Xuhui Wang,¹ Mairbek Chshiev,² and Aurelien Manchon^{1,*}

¹King Abdullah University of Science and Technology (KAUST),

Physical Science and Engineering Division, Thuwal 23955-6900, Saudi Arabia

²SPINTEC, UMR CEA/CNRS/UJF-Grenoble 1/Grenoble-INP, INAC, Grenoble, F-38054, France

(Dated: September 27, 2018)

In a ferromagnetic heterostructure, the interplay between a Rashba spin-orbit coupling and an exchange field gives rise to a current-driven spin torque. In a realistic device setup, we investigate the Rashba spin torque in the diffusive regime and report two major findings: (i) a nonvanishing torque exists at the edges of the device even when the magnetization and effective Rashba field are aligned; (ii) anisotropic spin relaxation rates driven by the Rashba spin-orbit coupling assign the spin torque a general expression $\mathbf{T} = T_{\parallel}^y(\theta)\mathbf{m} \times (\hat{\mathbf{y}} \times \mathbf{m}) + T_{\perp}^y(\theta)\hat{\mathbf{y}} \times \mathbf{m} + T_{\parallel}^z(\theta)\mathbf{m} \times (\hat{\mathbf{z}} \times \mathbf{m}) + T_{\perp}^z(\theta)\hat{\mathbf{z}} \times \mathbf{m}$, where the coefficients $T_{\parallel,\perp}^{y,z}$ depend on the magnetization direction. Our results agree with recent experiments.

PACS numbers: 75.60.Jk

The concept of current-driven spin-orbit torque in ultrathin ferromagnetic heterostructures^{1,2} and diluted magnetic semiconductors³ is attracting much attention for providing an efficient magnetization switch mechanism using just one ferromagnet. In contrast to the conventional spin-transfer torque that demands a spin-polarized current generated by a reference ferromagnet (polarizer),^{4,5} the spin-orbit torque accomplishes magnetization switching by transferring angular momentum between the spin and orbital degrees of freedom through a spin-orbit coupling. In ferromagnetic heterostructures typically made of magnetic trilayers comprising an ultrathin ferromagnetic film sandwiched between a noble metal and an insulator, experiments and theories have uncovered a spin-orbit torque of the form^{2,6,7}

$$\mathbf{T} = T_{\parallel}\mathbf{m} \times (\hat{\mathbf{y}} \times \mathbf{m}) + T_{\perp}\hat{\mathbf{y}} \times \mathbf{m}, \quad (1)$$

where \mathbf{m} is the magnetization direction and $\hat{\mathbf{y}}$ is the directional unit vector (see Fig. 1). Two components in Eq.(1) are usually referred to as *in-plane* (T_{\parallel}) and *perpendicular* (T_{\perp}) torques.

The current understanding of the origin of spin-orbit torque in ferromagnetic heterostructures combines spin-Hall effect⁸ and band structure-induced effects. In the former, a spin current is generated by the spin-Hall effect in the noble metal layer and injected into the ferromagnet to produce a torque.^{9,10} In the latter, symmetry breaking across the interface between the noble metal and the ferromagnet induces a spin splitting in the band structure, leading to a nonvanishing current-induced spin-orbit field. One version of this band structure-induced spin-orbit torque is the so-called Rashba torque¹ where an electric field \mathbf{E} embedded across the interface produces a nonequilibrium Rashba field $\mathbf{B}_R \propto \hat{\mathbf{z}} \times \mathbf{E}$. Recent works have emphasized the complexity of these torques as functions of materials parameters.¹¹ Of most interest to the present study, it has been shown that the spin-orbit torque possesses a complex angular dependence that is

not captured by the earlier models based on either spin-Hall effect or Rashba torques.¹²

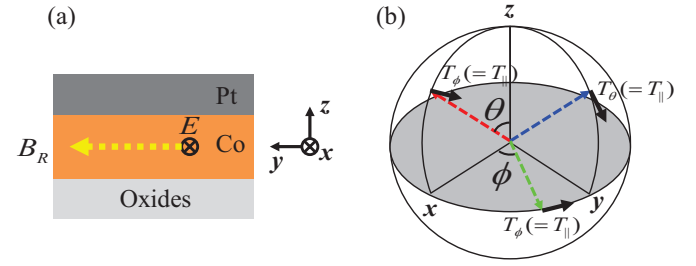


FIG. 1. (Color online)(a) Schematic view the device cross section. A charge current is flowing along the x direction, generating an effective Rashba field \mathbf{B}_R (dotted yellow line) that is pointing to y . L is the size of the lateral dimensions. (b) Spin torque components \mathbf{T}_ϕ and \mathbf{T}_θ in a spherical coordinate, with θ and ϕ being the azimuthal and the in-plane angle, respectively. The coordinates dashed lines show the magnetization directions considered in this Letter.

In this Letter, we employ a set of coupled spin-charge diffusion equations⁶ to characterize the Rashba spin torque in a square-shaped device with a width (and length) L , see Fig.1. We highlight two major findings. First, even when the magnetization \mathbf{m} is aligned along the effective spin-orbit field (along the $\hat{\mathbf{y}}$ direction), the spin-orbit torque does *not* vanish at the edges of the device. Second, the torque amplitudes vary with the magnetization direction (a behavior to be referred as *angular dependence*) and are size-dependent. In the weak (spin-orbit) coupling regime, the angular dependence vanishes as the device size increases; whereas in a strong coupling regime, the angular dependence is insensitive to the device size.

A schematic view of the device is shown in Fig. 1(a). The inversion asymmetry across the interfaces generates a Rashba type spin-orbit coupling from the potential gradient along the $\hat{\mathbf{z}}$ direction. In the *quasi-two-*

dimensional system considered here, the diffusive dynamics of nonequilibrium spin density \mathbf{S} and charge density n are described by^{6,13}

$$\frac{\partial n}{\partial t} = D\nabla^2 n + B\nabla_{xy} \cdot \mathbf{S} + \Gamma\nabla_{xy} \cdot \mathbf{m}n + R\nabla_{xy} \cdot \mathbf{m}(\mathbf{S} \cdot \mathbf{m}), \quad (2)$$

$$\begin{aligned} \frac{\partial \mathbf{S}}{\partial t} = & D\nabla^2 \mathbf{S} - \frac{\mathbf{S}}{\tau_{sf}} - \frac{\mathbf{S} + S_z \hat{\mathbf{z}}}{\tau_{DP}} - \frac{\mathbf{m} \times (\mathbf{S} \times \mathbf{m})}{T_{xc}} + B\nabla_{xy} n \\ & - \Delta_{xc} \mathbf{S} \times \mathbf{m} + 2C\nabla_{xy} \times \mathbf{S} + 2R(\mathbf{m} \cdot \nabla_{xy} n)\mathbf{m} \\ & + \Gamma[\mathbf{m} \times (\nabla_{xy} \times \mathbf{S}) + \nabla_{xy} \times (\mathbf{m} \times \mathbf{S})]. \end{aligned} \quad (3)$$

The parameters are: $\hbar = 1$, $C = \alpha v_F k_F \tau$, $\Gamma = \alpha \Delta_{xc} v_F k_F \tau^2 / 2$, $R = \alpha \Delta_{xc}^2 \tau^2 / 2$, and $B = 2\alpha^3 k_F^2 \tau^2$. α denotes the Rashba spin-orbit coupling and $\nabla_{xy} = \hat{\mathbf{z}} \times \nabla$. The momentum relaxation time is τ and spin relaxation time due to magnetic impurities is given phenomenologically by τ_{sf} , whereas $\tau_{DP} = 1/2\alpha^2 k_F^2 \tau$ is the D'yakonov-Perel relaxation time.¹⁴ $k_F(v_F)$ is the Fermi momentum (velocity) while $D = v_F^2 \tau / 2$ is the diffusion constant. Briefly, Δ_{xc} - and C -terms describe spin precession around the exchange field and \mathbf{B}_R , respectively. B -term couples spin and charge degrees of freedom, leading to the electrical spin generation and spin-Hall effect. Γ -term provides a higher order correction to the precessional motion described by first two terms. R -term contributes to a magnetization renormalization. $T_{xc} = 1/\Delta_{xc}^2 \tau$ is the transverse spin dephasing time in the limit of a weak ferromagnet.¹⁵ As a boundary condition suggested by experiments,¹⁶ the nonequilibrium spin density is required to vanish at the transverse edges along the y direction.

In a recent work, it was shown that reducing the width of the magnetic film dramatically modifies the relative magnitude of the in-plane and perpendicular torques in the weak Rashba limit.⁶ Here, we further argue that reducing the size of the device results in changes in the symmetry of the torque. To support our argument, we plot in Fig. 2 the spatial distribution of the spin torque density (along the y axis in the yz -plane) for various magnetization directions in both weak ($\Delta_{xc} \gg \alpha k_F$) and strong ($\Delta_{xc} \ll \alpha k_F$) spin-orbit coupling regimes. In Fig. 1(b), the spin torque density is expressed in spherical coordinates, $\mathbf{T} = T_\phi \hat{\mathbf{e}}_\phi + T_\theta \hat{\mathbf{e}}_\theta$, which is more general than Eq. (1). On the right column of Fig. 2, T_θ is robust in the bulk, resulting from a robust nonequilibrium spin density (S_y) driven by the spin-galvanic effect discussed by Edelstein.¹⁷ This effect disappears towards the boundaries, as imposed by the boundary conditions.¹⁶

An important feature in Fig. 2 appears to be the non-vanishing spin torque at the edges even when the magnetization \mathbf{m} is parallel to \mathbf{B}_R (deep blue curves). In general, as the angle between the exchange field \mathbf{m} and \mathbf{B}_R closes, the spin torque amplitude decreases. For a strong spin-orbit coupling, the spin-Hall effect drives oppositely polarized spin densities S_z accumulating at opposite edges.⁸ In our finite-size device, within the distance of spin-flip relaxation length from the edges, the

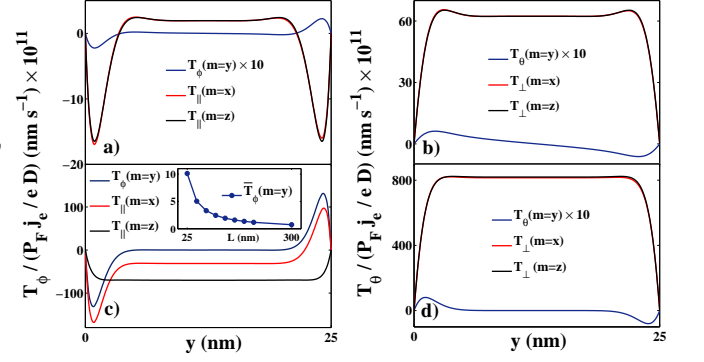


FIG. 2. (Color online) Spatial distribution of the Rashba torque along the y axis, for a device $L = 25$ nm. The yz -plane is located at the center of the device, i.e., $x = 12.5$ nm. Panels (a) and (c) refer to the *in-plane* component (here $T_{\parallel} \equiv T_{\phi}$). Panels (b) and (d) are for the *out-of-plane* component ($T_{\perp} \equiv T_{\theta}$). Panels (a) and (b): weak Rashba regime ($\alpha = 0.001$ eV nm, $\Delta_{xc} = 0.1$ eV). Panels (c) and (d): strong coupling ($\alpha = 0.05$ eV nm, $\Delta_{xc} = 0.01$ eV). The inset in panel (c) displays: $\bar{T}_{\phi(m=y)} = \int_{y=L/2}^{y=L} T_{\phi(m=y)} dy / L$ for different widths. In panels (a),(b) and (d), $T_{\phi(m=y)}$ is multiplied by a factor 10. The Fermi energy is $E_F = 0.7$ eV, $k_F = 4.3$ nm⁻¹ and $v_F = 5 \times 10^{14}$ nm s⁻¹. $\tau = 10^{-15}$ s and $\tau_{sf} = 10^{-12}$ s.

spin density S_z distributed along the y direction generates a nonvanishing local spin torque (at the edges) when \mathbf{m} is parallel to \mathbf{B}_R . As the spin-orbit coupling weakens, torques at $\mathbf{m} \parallel \mathbf{B}_R$ driven by the spin-Hall effect become negligible, see Fig.2(a). Meanwhile, as the sample size increases $L \gg \lambda_{sf}$, the expression $\bar{T}_{\phi(m=y)} = (1/L) \int_{y=L/2}^{y=L} T_{\phi(m=y)} dy$ exponentially decreases, see inset in Fig. 2(c). Another important feature is the inhomogeneous profile of T_{ϕ} , which is driven by the competing effects of spin precession around the total field and spin Hall-effect: the spin-Hall effect (precession around the total field) is dominant in the strong (weak) Rashba regime. When $\mathbf{m} = \hat{\mathbf{z}}$, spin density S_z does not contribute to the spin-Hall induced torque and the in-plane torque becomes homogeneous, as confirmed by the solid black line in Fig.2(c). In a finite size device, these effects contribute to the angular dependence discussed in the following.

First, in an infinite system with a weak Rashba spin-orbit coupling, once the anisotropy in spin relaxation rates due to the D'yakonov-Perel mechanism is quenched, Eq. (3) gives rise to a torque described by Eq. (1).⁶ However, as long as the spin relaxation rate is not isotropic, the torque assumes a more complex angular dependence. In an infinite system, setting $\nabla_{xy} = \hat{\mathbf{z}} \times eE\partial_{\epsilon}\hat{\mathbf{x}}$, Eq. (3) reduces to

$$\begin{aligned} \Delta_{xc} \mathbf{S} \times \mathbf{m} + \frac{1}{T_{xc}} \mathbf{m} \times (\mathbf{S} \times \mathbf{m}) \\ + \frac{1}{\tau_{xy}} S_x \hat{\mathbf{x}} + \frac{1}{\tau_{xy}} S_y \hat{\mathbf{y}} + \frac{1}{\tau_z} S_z \hat{\mathbf{z}} = \mathbf{X}, \end{aligned} \quad (4)$$

where the last three terms on the left-hand side subscribe to both the D'yakonov-Perel mechanism and spin relaxation induced by random magnetic impurities: $\tau_{xy}^{-1} = \tau_{DP}^{-1} + \tau_{sf}^{-1}$ and $\tau_z^{-1} = 2\tau_{DP}^{-1} + \tau_{sf}^{-1}$. On the right-hand side, the source term reads

$$\mathbf{X} \equiv \frac{nE}{\epsilon_F} (B\hat{\mathbf{y}} + 2CP\hat{\mathbf{y}} \times \mathbf{m} + \Gamma P\mathbf{m} \times (\hat{\mathbf{y}} \times \mathbf{m})), \quad (5)$$

where P is the spin polarization at Fermi level (ϵ_F). Equation (4) can be analytically solved in spherical coordinates using $\mathbf{T} = T_\phi \hat{\mathbf{e}}_\phi + T_\theta \hat{\mathbf{e}}_\theta$. In the strong coupling limit ($B \gg C, \Gamma$), the spin torque becomes

$$\begin{aligned} \mathbf{T} = \frac{BnE}{\epsilon_F} \epsilon_\theta & [\beta \hat{\mathbf{y}} \times \mathbf{m} + (1 + (\xi - \beta)\xi) \mathbf{m} \times \hat{\mathbf{y}} \times \mathbf{m} \\ & - \chi(1 - \alpha_\theta \cos^2 \theta) (\mathbf{m} \cdot \hat{\mathbf{x}}) \mathbf{m} \times \hat{\mathbf{z}} \times \mathbf{m} \\ & - \alpha_\theta m_z m_y (1 + (\xi - \beta)\xi) \mathbf{m} \times \hat{\mathbf{z}} \times \mathbf{m} \\ & + \chi(\xi - \beta)(1 - \alpha_\theta \cos^2 \theta) (\mathbf{m} \cdot \hat{\mathbf{x}}) \hat{\mathbf{z}} \times \mathbf{m} \\ & - \beta \alpha_\theta m_z m_y \hat{\mathbf{z}} \times \mathbf{m}], \quad (6) \end{aligned}$$

which comprises one of the major results of this Letter. For a succinct discussion, the parameters in Eq.(6) are defined in Ref.18.

Equation (6) contains both odd and even components with respect to the inversion of magnetization direction (\mathbf{m}), which agrees with the expressions proposed by Garello *et al* [see Eqs.(9) and (10) in Ref. 12]. In particular, besides the regular *in-plane* and *perpendicular* torques captured by Eq. (1), additional terms in the form of $\hat{\mathbf{z}} \times \mathbf{m}$ and $\mathbf{m} \times (\hat{\mathbf{z}} \times \mathbf{m})$ arise. The relative magnitude of the different contributions depends on the materials parameters. Furthermore, it is interesting to notice that such a complex angular dependence of the torque is solely determined by the anisotropy in spin-relaxation rates (times). By suppressing the anisotropy, i.e., $\tau_z = \tau_{xy}$ and $1/\tau_- = 0$, the torque reduces to

$$\mathbf{T} = \frac{BnE}{\epsilon_F} \left[\frac{\beta}{1 + \xi^2} \hat{\mathbf{y}} \times \mathbf{m} + \left(1 - \frac{\beta\xi}{1 + \xi^2} \right) \mathbf{m} \times \hat{\mathbf{y}} \times \mathbf{m} \right], \quad (7)$$

[see Eq.(1)] and the complex angular dependence vanishes. In our model, this anisotropic spin relaxation is determined by the D'yakonov-Perel mechanism arising from scatterings in the presence of Rashba spin-orbit coupling.¹⁴ We emphasize here that the above analytical results are obtained in a sample of infinite size in the strong Rashba coupling regime.

In the following, we show that the angular dependence of the Rashba torque shown in Eq. (6) also exists in a device of *finite* size. In addition, we also explain the symmetry properties of spin torque at sample edges, as shown in Fig. 3. We analyze the angular dependence for various \mathbf{m} in the xz -plane at three particular locations in the device, i.e., in the center (at $x, y = 12.5$ nm) to represent bulk values, and two other locations near the edges along y (at $x = 12.5$ nm). In what follows, the

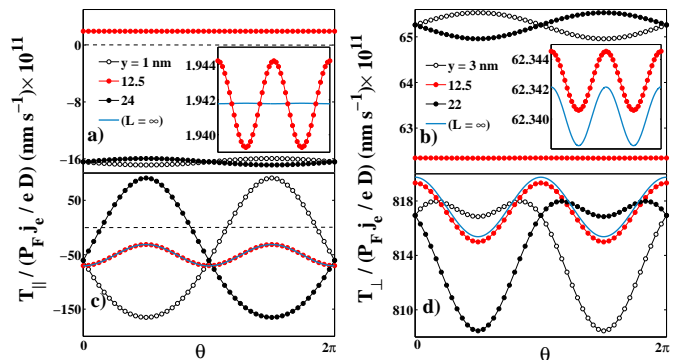


FIG. 3. (Color online) Angular dependence of spin torque as \mathbf{m} varies in the xz -plane in a system with $L = 25$ nm. Panels (a) and (c): in-plane torque; panels (b) and (d): out-of-plane component. Panels (a) and (b): weak Rashba regime; panels (c) and (d): strong Rashba regime. Solid red curves are taken at the center of the device. Empty and solid black dots are taken at positions near two boundaries along the y direction. Insets in panels (a),(b) give a better picture of the solid red curves. Solid cyan lines refer to the spin torque for $L = \infty$.

description is taken considering T_{\parallel} and T_{\perp} , defined in Eq. (1).

In the weak Rashba regime, when the magnetization is along $\hat{\mathbf{z}}$, the spin density components that contribute to the torque show a symmetric profile.⁶ As \mathbf{m} moves towards the $\hat{\mathbf{x}}$ axis, the spin density generated perpendicular to $(\mathbf{m}, \mathbf{B}_R)$ points to the $\hat{\mathbf{z}}$ direction. However, the faint presence of spin-Hall effect still renders the total profile asymmetric, i.e., one edge is more negative than the other, in contrast to the case when $\mathbf{m} = \hat{\mathbf{z}}$. Such an effect contributes to the angular dependence at the edge of the device, as depicted by the open and filled black dots in Fig.3(a)(b). In the strong Rashba regime, the spin-Hall effect is dominating, producing a more pronounced angular dependence, as shown by the open and filled black dots in Fig.3(c)(d).

To illustrate the above effects when magnetization is in the xz -plane, we study the angular dependence in the bulk for different device sizes (in Fig. 3, $L = 25$ nm and $L = \infty$, only). In the strong Rashba regime, the spin relaxation rate is dominated by D'yakonov-Perel term, the angular dependence is pronounced and it does not change as the device size increases, which shall eventually approach the limit characterized by Eq.(6). In contrast, in the weak Rashba regime the relaxation rate is mostly isotropic, which results in a weak angular dependence that vanishes as the size increases. These numerical results are consistent with the argument that the angular dependence of spin torque in the bulk is driven by the anisotropy in spin relaxation rate. Furthermore, in a finite system with isotropic spin relaxation rates, oscillations may arise due to edge effects diffusing towards the center and such a phenomenon is better seen in the weak Rashba regime [see inset in Fig. 3(a)]. In Fig. 4, the spin torque density in the bulk is plot-

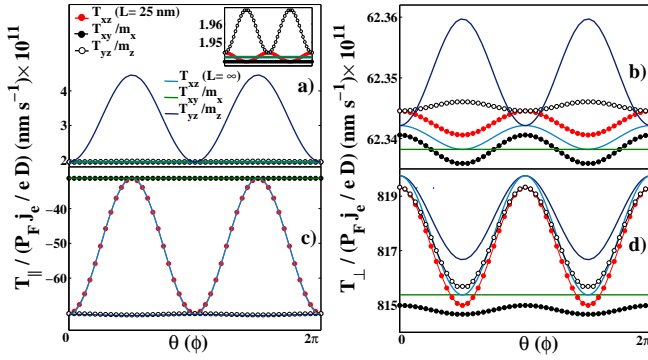


FIG. 4. (Color online) Angular dependence as \mathbf{m} varies in the xz , xy and yz planes in the center of the system for $L = 25$ nm and $L = \infty$. Panels (a) and (c): in-plane torque; panels (b) and (d): out-of-plane component. Panels (a) and (b) weak Rashba regime; panels (c) and (d) strong Rashba regime. T_{ij} refers to the spin torque in the ij - plane. The spin torque is divided by $m_x = \cos \phi$ ($m_z = \cos \theta$) in the xy - (yz -) plane.

ted when \mathbf{m} rotates in the xz -, xy - and yz - planes. For the latter two planes, the angular dependence coming from the cross product in Eq. 1 is removed (division by $\cos \phi(\cos \theta)$). Therefore, the oscillations of the torque magnitude in these three cases can be fitted by $K_1 + K_2 \sin^2 \phi(\sin^2 \theta) + K_3 \sin^4 \phi(\sin^4 \theta)$, which is con-

sistent with Eq. (6). A prominent feature is that the oscillations in the xy -plane vanish as the device size increases; whereas in the yz -plane, the oscillations persist even with an isotropic relaxation rate, which is due to Γ -term contributing to the angular dependence when \mathbf{m} is in the yz -plane, thus enhancing the spin torque amplitude in the weak Rashba regime [see Fig. 4(a)(b)].

In conclusion, for a finite-size Rashba torque device, we have shown that the spin torque is nonvanishing at the edges of the sample even when the magnetization and the effective Rashba field are parallel, as a result of the competition between spin-Hall effect and the nonequilibrium spin density generated due to anisotropic spin relaxation rates. Furthermore, the symmetry and angular dependence of the spin torque are in general more complicated than the conventional form assumed to date. In our calculations, the angular dependence is much larger for T_{\parallel} than for T_{\perp} . For a sample of an infinite size, we have obtained an analytical expression for the spin-orbit torque that shows both odd and even components against magnetization inversion and agrees favorably with the expression proposed based on experimental results. In a view of increasing industrial and academic interests in the field of spin-orbit torques, we expect that results presented in this Letter shall not only provide a better understanding to the key mechanisms behind the experimental observations but also shed light on the design of realistic devices.

We thank I. M. Miron, K. Garello, K. -J. Lee, P. M. Haney and M. D. Stiles for valuable discussions.

* aurelien.manchon@kaust.edu.sa

- ¹ A. Manchon and S. Zhang, Phys. Rev. B **78**, 212405 (2008); Phys. Rev. B **79**, 212405 (2009); I. Garate and A. H. MacDonald, Phys. Rev. B **80**, 134403 (2009); A. Matos-Abiad and R. L. Rodriguez-Suarez, Phys. Rev. B **80**, 094424 (2009).
- ² I. M. Miron *et al.*, Nature Mater. **9**, 230 (2010); U. H. Pi *et al.*, Appl. Phys. Lett. **97**, 162507 (2010); I. M. Miron, *et al.*, Nature (London) **476**, 189 (2011).
- ³ A. Chernyshov, *et al.*, Nature Phys. **5**, 656 (2009); D. Fang, *et al.*, Nature Nanotech. **6**, 413 (2011); K. M. D. Hals, A. Brataas and Y. Tserkovnyak, Europhys. Lett. **90**, 47002 (2010).
- ⁴ J. C. Slonczewski, J. Magn. Magn. Mater. **159**, L1 (1996); L. Berger, Phys. Rev. B **54**, 9353 (1996).
- ⁵ D. C. Ralph and M. D. Stiles, J. Magn. Magn. Mater. **320**, 1190 (2008), and references therein.
- ⁶ X. Wang and A. Manchon, Phys. Rev. Lett. **108**, 117201 (2012).
- ⁷ K.-W. Kim *et al.*, Phys. Rev. B **85** 180404(R) (2012); D. A. Pesin and A. H. MacDonald, Phys. Rev. B **86** 014416 (2012); E. van der Bijl and R. A. Duine, Phys. Rev. B **86**, 094406 (2012).
- ⁸ J. E. Hirsch, Phys. Rev. Lett. **83**, 1834 (1999); S. Zhang, Phys. Rev. Lett. **85**, 393 (2000).

- ⁹ L. Liu *et al.*, Phys. Rev. Lett. **109**, 096602 (2012); L. Liu *et al.*, Science **336**, 555 (2012).

¹⁰ P.M. Haney *et al.*, , arXiv:1301.4513

¹¹ J. Kim *et al.*, , Nature Materials **12**, 240 (2013).

¹² K. Garello, *et al.*, arXiv:1301.3573

¹³ X. Wang, C. Ortiz Pauyac, and A. Manchon, arXiv:1206.6726, (2012).

¹⁴ M. I. D'yakonov and V. I. Perel, Sov. Phys. JETP Lett. **13**, 467 (1971).

¹⁵ C. Petitjean, D. Luc, and X. Waintal, Phys. Rev. Lett. **109** 117204 (2012); Y. Tserkovnyak, A. Brataas, and G. E. W. Bauer, J. Magn. Magn. Mater. **320**, 1282 (2008).

¹⁶ Y. K. Kato, *et al.*, Science **306**, 1910 (2004).

¹⁷ V. M. Edelstein, Solid State Commun. **73**, 233 (1991).

¹⁸ Here, we provide the parameters used in Eq.(6)

$$\epsilon_{\theta} = [1 + \xi^2 + \xi \chi \sin^2 \theta (1 - \alpha_{\theta} \cos^2 \theta)]^{-1}, \quad (8)$$

$$\alpha_{\theta} = \frac{\tau_{\parallel}(\theta)}{\tau_{-}}, \quad \frac{1}{\tau_{\parallel}(\theta)} = \frac{1}{\tau_{xy}} + \frac{\cos^2 \theta}{\tau_{-}} \quad (9)$$

where $\xi = \frac{\tau_{\Delta}}{\tau_{+}}$, $\beta = \frac{\tau_{\Delta}}{\tau_{xy}}$, $\chi = \frac{\tau_{\Delta}}{\tau_{-}}$, $\tau_{\Delta} = \frac{1}{\Delta_{xc}}$, $\frac{1}{\tau_{+}} = \frac{1}{T_{xc}} + \frac{1}{\tau_{xy}}$, and $\frac{1}{\tau_{-}} = \frac{1}{\tau_{z}} - \frac{1}{\tau_{xy}}$.